ELSEVIER

Journal of Fluids and Structures 26 (2010) 611–625

JOURNAL OF FLUIDS AND STRUCTURES

www.elsevier.com/locate/jfs

Experimental investigation of flow-induced vibration on isolated and tandem circular cylinders fitted with strakes ☆

I. Korkischko*, J.R. Meneghini

NDF, Department of Mechanical Engineering, POLI, University of São Paulo, Brazil

Received 3 April 2009; accepted 25 February 2010
Available online 15 April 2010

Abstract

The effect of varying the geometric parameters of helical strakes on vortex-induced vibration (VIV) is investigated in this paper. The degree of oscillation attenuation or even suppression is analysed for isolated circular cylinder cases. How a cylinder fitted with strakes behaves when immersed in the wake of another cylinder in tandem arrangement is also investigated and these results are compared to those with a single straked cylinder. The experimental tests are conducted at a circulating water channel facility and the cylindrical models are mounted on a low-damping air bearing elastic base with one degree-of-freedom, restricted to oscillate in the transverse direction to the channel flow. Three strake pitches (p) and heights (h) are tested: $p = 5$, 10, $15d$, and $h = 0.1$, 0.2, $0.25d$. The mass ratio is 1.8 for all models. The Reynolds number range is from 1000 to 10 000, and the reduced velocity varies up to 21. The cases with $h = 0.1d$ strakes reduce the amplitude response when compared to the isolated plain cylinder, however the oscillation still persists. On the other hand, the cases with $h = 0.2$, $0.25d$ strakes almost completely suppress VIV. Spanwise vorticity fields, obtained through stereoscopic digital particle image velocimetry (SDPIV), show an alternating vortex wake for the $p = 10d$ and $h = 0.1d$ straked cylinder. The $p = 10d$ and $h = 0.2d$ cylinder wake has separated shear layers with constant width and no roll-up close to the body. The strakes do not increase the magnitude of the out-of-plane velocity compared to the isolated plain cylinder. However, they deflect the flow in the out-of-plane direction in a controlled way, which can prevent the vortex shedding correlation along the span. In order to investigate the wake interference effect on the strake efficiency, an experimental arrangement with two cylinders in tandem is employed. The centre-to-centre distance for the tandem arrangement varies from 2 to 6. When the downstream $p = 10d$ and $h = 0.2d$ cylinder is immersed in the wake of an upstream fixed plain cylinder, it loses its effectiveness compared with the isolated case. Although the oscillations have significant amplitude, they are limited, which is a different behaviour from that of a tandem configuration with two plain cylinders. For this particular case, the amplitude response monotonically increases for all gaps, except one, a trait usually found in galloping-like oscillations. SDPIV results for the tandem arrangements show alternating vortex shedding and oscillatory wake.

Keywords: Vortex-induced vibration; Helical strakes; Tandem arrangement; Flow interference; Stereoscopic DPIV

☆ funded by BZG.
*Corresponding author. Tel.: +55 11 3091 5724; fax: +55 11 3091 5642.
E-mail address: ivan.korkischko@poli.usp.br (I. Korkischko).

0889-9746/$ - see front matter © 2010 Elsevier Ltd. All rights reserved.
doi:10.1016/j.jfluidstructs.2010.03.001

1. Introduction

The flow around bluff bodies, together with the associated vortex-induced vibration (VIV), are subjects of research by both academia and industry, given their theoretical and applied importance. The fluid-structure interaction, with special interest to the circular cylinder geometry, has been extensively reviewed by Sarpkaya (1979), Bearman (1984), Parkinson (1989), Khalak and Williamson (1999), and Williamson and Govardhan (2004). The vortex shedding present in flows with Reynolds number above 46 results in oscillating longitudinal and transverse forces, drag and lift, respectively, acting on the circular cylinder. When the vortex shedding frequency is close to the structural frequency, the structure can oscillate at very high amplitudes. This oscillation is usually named vortex-induced vibration. Because the persisting oscillations may lead to fatigue failure, a subject of great interest for industry, the VIV phenomenon can be very damaging to some structures including chimney stacks, cables, and risers.

Flow interference between cylinders also has great research interest since it is responsible for several changes in the characteristics of fluid load. The tandem arrangement of two circular cylinders can be extrapolated to represent the basic flow characteristics of interference between different structures. Classifying the different flow regimes based on the gap (s/d) was proposed by Zdravkovich (1985). Previous investigations of tandem configurations by Brika and Laneville (1999), Laneville and Brika (1999), Hover and Triantafyllou (2001), Alam et al. (2003) and Ássi et al. (2006) showed substantial complexity in fluid dynamics as the spacing between the cylinders is varied, including a combination of vortex-induced vibration and galloping-like oscillations. When the upstream cylinder is fixed and the downstream cylinder is free to oscillate, both vortex resonance and the occurrence of wake-galloping instability are equally possible and can occur separately or combined depending on the separation distance according to Bokaian and Geoola (1984).

Although the staggered and the side-by-side arrangements are not the subjects of this paper, they received special attention in recent experimental studies conducted by Sumner et al. (2000), Li and Sumner (2009) and Hanson et al. (2009). These two arrangements, along with the tandem configuration, display significant differences from the fluid characteristics of the flow around an isolated cylinder.

In this context, the control of flow over a bluff body is introduced in order to reduce the amplitude of the oscillating forces and displacements. Choi et al. (2008) classify the methods of flow control as passive, active open-loop and active closed-loop. Special attention has been paid to passive control because, among the three different groups, passive control is the easiest to implement in experiments, but it usually requires an initial parametric study for a successful control result. Different passive control methods to suppress vortex shedding and VIV have been studied by Bearman and Owen (1998), Galvao et al. (2008), Ássi et al. (2009), and reviewed by Zdravkovich (1981). Among the various geometrical forms of devices for passive suppression, helical strakes are some of the most common in both air and water flows, as can be seen in chimneys and offshore structures, such as risers and spars. Experimental studies about the effectiveness of strakes were performed by Simantiras and Willis (1999), Bearman and Branković (2004), Trim et al. (2005), Branković and Bearman (2006) and Korkischko et al. (2007b). Strakes can effectively suppress VIV, depending on pitch and height parameters at the expense of drag increase. The VIV suppression of strakes is widely understood to be a combination of two effects: strakes prevent the shedding from becoming correlated along the span and the three-dimensionality of the separating flow created by the strakes destroys regular vortex shedding.

As expected, the interference affects the characteristics of flow around the straked cylinders. Zdravkovich (1984) showed the adverse effect of interference in the effectiveness of strakes in suppressing VIV. More recently, Korkischko et al. (2007a) demonstrated that strakes lose their effectiveness when a downstream straked cylinder elastically mounted is immersed in the wake of an upstream plain fixed cylinder at $s/d = 3.4$ centre-to-centre distance.

Numerical simulations become more feasible with the development of numerical methods and the increase of computational power. Studies on an isolated plain cylinder (Willden and Graham, 2001), tandem interference (Carmo and Meneghini, 2006; Papaioannou et al., 2008; Prasanth and Mittal, 2009; Carmo et al., 2010), side-by-side (Mizushima and Ino, 2008), tandem and side-by-side interference (Meneghini et al., 2001), staggered arrangement (Carmo et al., 2008), plain and wired cylinders (Rocchi and Zasso, 2002), and straked cylinders (Constantinides and Oakley, 2006) are just a few examples of numerical simulation studies within the scope of this paper.

On the other hand, experimental studies are still necessary to validate numerical simulations. This paper presents measurements of vortex-induced vibrations of a single cylinder in order to validate the experimental set-up and to serve as a basis of comparison for the other tests. Firstly, the assessment of the strake effectiveness and its hydrodynamic characteristics is made by varying the main strake geometric parameters (pitch and height). Then, the plain cylinder tandem arrangement is investigated to identify the changes in flow dynamics and the galloping phenomena. Finally, employing the plain cylinder tandem arrangement as a basis of comparison, the plain/straked cylinder tandem arrangement is investigated in order to ascertain the fluid-flow mechanisms that reduce the effectiveness of the strakes in this condition. The chosen pitch, height and tandem separation are typical values found in industrial applications, specially those employed by the offshore industry; as such, they are commonly found in other studies, which form a

convenient basis of comparison. The Reynolds number range was limited by the dimensional and operational characteristics of the experimental arrangement. The structural response is obtained through time histories of amplitude and the fluid dynamics are analysed through vorticity and velocity fields acquired by stereoscopic digital image velocimetry (SDPIV). This technique is described in detail in (Prasad, 2000). In the SDPIV technique, the use of two views contains sufficient information to extract the out-of-plane motion of particles and removes the perspective error which can corrupt the in-plane measurement.

With the intention of investigating the effectiveness of strakes acting as VIV suppressors, in addition to the effect of its two main geometric parameters (pitch and height), we present amplitude and frequency responses, as well as SDPIV spanwise vorticity and velocity fields. The SDPIV measurements are carried out in order to characterize the flow around isolated plain and straked cylinders. Different combinations of pitches and heights are employed to obtain the most effective configurations regarding the VIV suppression. Additionally, the tandem configuration is investigated because it leads to very different characteristics of flow and response for both downstream plain and straked cylinders. For example, a straked cylinder that does not develop VIV when it is isolated oscillates at significant amplitudes when it is immersed in the wake of an upstream fixed plain cylinder. This behaviour is not desired since strakes can be fitted in structures that are arranged in interference configurations.

2. Experimental arrangement

The experimental tests were conducted at the Fluid-Dynamics Research Group Laboratory (NDF) of the University of São Paulo (USP). The circulating water channel facility has a $0.70 \times 0.80 \times 7.50$ m test-section. The flow velocity can be increased up to 1.0 m/s. The channel operates at a low turbulence level ($<2\%$). Additional information about the experimental facility can be found in Ássi (2005) and Ássi et al. (2006).

The rigid acrylic circular cylinders have a diameter $d = 32$ mm and an immersed length of $l = 790$ mm, giving an aspect ratio $l/d = 24.7$. The strakes are made of rigid rubber and a set of three pitches (p): $5d$, $10d$, and $15d$, and three heights (h): $0.1d$, $0.2d$, and $0.25d$, is tested. The straked cylinders have a three-start helical pattern configuration and thin plate geometry as depicted in Fig. 1. The strakes are attached to the cylinders using a cyanoacrylate adhesive and the cylinders are fitted with end-plugs to ensure complete water-tightness. Seven straked models are tested in the isolated cylinder arrangement: 5/0.1 (pitch $p = 5d$, and height $h = 0.1d$), 5/0.2 ($p = 5d$, and ($h = 0.2d$), 10/0.1 ($p = 10d$, and $h = 0.1d$), 10/0.2 ($p = 10d$, and $h = 0.2d$), 10/0.25 ($p = 10d$, and $h = 0.25d$), 15/0.1 ($p = 15d$, and $h = 0.1d$), and 15/0.2 ($p = 15d$, and $h = 0.2d$). In the interference tests, the upstream cylinder is fixed and plain, and the downstream one is elastically mounted and either plain or straked (10/0.2). The tandem arrangement (Fig. 2(a)) has centre-to-centre cylinder distances $s/d = 2,3,4,5$ and 6.

The cylinders are rigidly attached beneath a platform on an elastic air-bearing system that allows motion only in a direction transverse to the flow, as shown in Fig. 2(b). Transverse motion is measured by a Leuze (OSDL 8/V4) laser position sensor, transverse acceleration by a Kistler (8305B2M2SP5M) accelerometer, and flow velocity by a Siemens (Sitrans F M Magflo MAG5000) electromagnetic flowmeter. Data acquisition is performed by a National Instruments system. The sampling rate is 100 Hz during a 120 s time interval. Each data point contains at least 30 oscillation cycles,

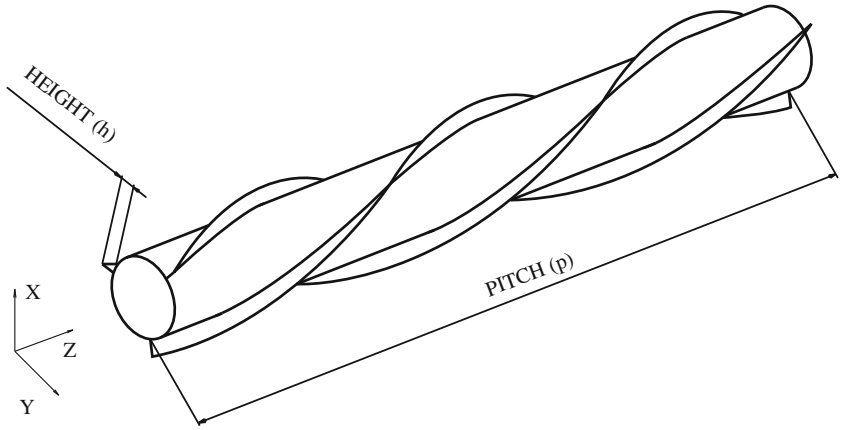

Fig. 1. Circular cylinder fitted with helical strakes.

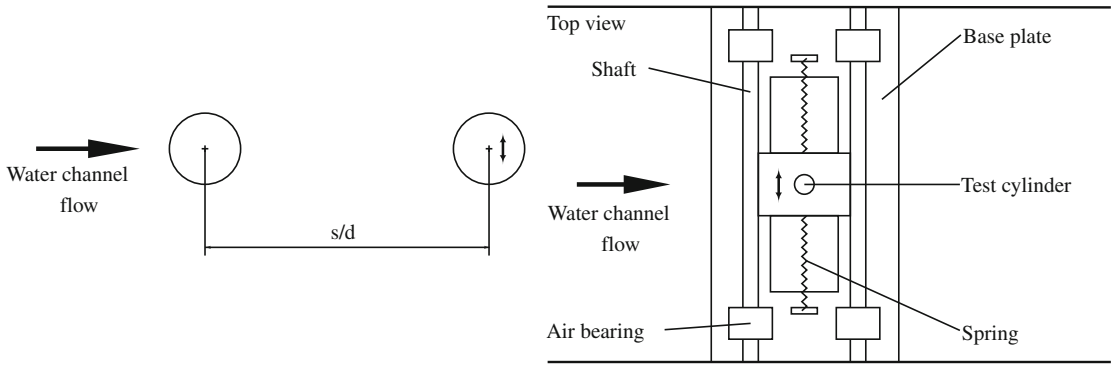

(a) Tandem arrangement. (b) Schematic of the air bearing system.

Fig. 2. Schematics of the experimental arrangement.

considering that the lowest measured oscillation frequency is $f \approx 0.25$ Hz. The time interval between measurements is 120 s to assure a proper stabilization of the flow in the water channel.

The end conditions of the cylinders are free surface at the upper end and near wall at the bottom. The gap between the model tip and the bottom of the water channel is about 10 mm. Due to this very small gap, an end-plate was not necessary. Considering the high aspect ratio of the models, the end effects are restricted to a small region. For this water channel, Ássi (2005) found a maximum variation of 5% for the mean value of the velocity profile. Hence, as the flow velocity ranges from 0.03 to 0.30 m/s, the free surface is expected not to affect the overall results. The structure supporting the air-bearing base is fixed above the circulating water channel.

In all tests, the mass parameter ($m^* = 4m/\pi\rho d^2 l$, where m is the moving structural mass) is $m^* = 1.8$. The mass parameter is the ratio between the moving structural mass and the displaced fluid mass. The structural damping coefficient in air is $\zeta = 0.0045$, leading to a mass-damping parameter $m^*\zeta = 0.0081$.

The Reynolds number is in the range of 1000–10 000, and the reduced velocity varies from 3 to 21. The reduced velocity is defined as $V_r = U/f_n d$, where U is the water channel flow velocity, f_n is the natural frequency in still water, and d is the diameter of the plain cylinder. The natural frequency f_n is obtained through decay tests in still water, while the structural damping coefficient is obtained from decay tests performed in air.

The SDPIV images are obtained by seeding the liquid with polyamide particles about 11 μm in diameter. A Quantel (Brilliant Twins) double-cavity pulsed Nd:YAG laser with a 532 nm wavelength illuminates the flow. A workstation, the DaVis 7.2 software and two Imager Pro X 2 Megapixel cameras compose the LaVision FlowMaster 3D-Stereo PIV system. Two Nikon (AF Nikkor f/1.4D) lenses of 50 mm focal length are used in the stereoscopic measurements. The SDPIV velocity fields are measured at a rate of 15 Hz and at half the distance of the immersed span. The acquisition rate is well beyond double the Strouhal and oscillation frequencies, therefore respecting the Nyquist theorem. The vector calculation employs a two-pass windowing process with decreasing size: the first correlation uses a 64×64 pixel interrogation window followed by the second correlation with a 32×32 pixel window. The field of view is $6.3 \times 4.6d$, resulting in a 102×75 point grid. Each SDPIV data set contains 345 vector fields that are sampled for 23 s. This is the maximum number of vector fields that can be measured due to the capacity of the camera storage. The spanwise vorticity and velocity fields are phase averaged employing at least 8 samples. A convergence test guarantees the validity of phase averaging with 8 cycles. The phase averaging uses one vector field for each oscillation cycle which is pinpointed at the same phase angle ϕ. This angle corresponds to the leftmost position during the cycle in the SDPIV figures. As noted by Govardhan and Williamson (2000), the phase averaging is useful to obtain clearer pictures of the spanwise vorticity and velocity fields of the flow, without smaller and weaker structures developing as a result of intermittent small-scale three-dimensionalities, mainly at the high Reynolds numbers (Re = 1000–10 000) present in this study.

3. Results

The dynamic response of the cylindrical models is presented in terms of the nondimensional amplitude ratio, $A^* = A/d$, and the nondimensional frequency ratio, $f^* = f/f_n$, versus the reduced velocity, V_r. Amplitudes are calculated by taking the average of the 10% highest peaks for each test.

Fields of nondimensional phase averaged spanwise vorticity, $\omega_z d/U_\infty$, and velocity, U_z/U_∞, measured by SDPIV are presented. The area of interest is the wake region of the oscillating cylinder. The spanwise vorticity, ω_z, is given by

$$\omega_z = \frac{\partial U_y}{\partial x} - \frac{\partial U_x}{\partial y}. \tag{1}$$

3.1. Isolated cylinders

In this subsection, the results for isolated plain and straked cylinders are presented in order to provide a reference to which the tandem arrangement results presented in the next subsection are compared.

Fig. 3 presents the amplitude response for an isolated plain cylinder that is elastically mounted and free to oscillate in the transverse (cross-flow) direction. The data compiled by Khalak and Williamson (1999) is shown along with the present data in order to compare close values of the mass parameter m^*. Although the parameters from the two experiments are not exactly the same, there is remarkable agreement between the two data sets. These are well-known results from the literature, where the initial, upper and lower branches, and the desynchronization region can be clearly seen. Williamson and Govardhan (2004) present a very detailed review about the synchronization regime.

Using the plain cylinder response as a basis of comparison, the main geometric parameters of strakes, pitch and height, are varied to investigate their effect on the response of cylinders fitted with strakes. Fig. 4(a) shows the importance of the strake height to VIV attenuation/suppression. The low-height $h = 0.1d$ strakes have a moderate effect in VIV attenuation. The increase in pitch reduces the maximum amplitude response and delays the beginning of the maximum amplitude range. All $h = 0.1d$ configurations display a desynchronization region that starts with a similar V_r compared to the plain cylinder case. For the high-height ($h = 0.2$, $0.25d$) configurations, the transverse oscillations have been almost completely suppressed, with no apparent differences between the three pitches and two heights tested. Similar results are found in experimental tests conducted by other researchers. The low-height strakes: 5/0.12 (Bearman and Branković, 2004), 5/0.14 (Trim et al., 2005), and 5/0.1 (Branković and Bearman, 2006) are not sufficient to suppress VIV, reducing the maximum amplitude by 50–60% compared to the plain cylinder. In accordance with the data presented in this paper, the transverse response is almost suppressed for the high-height strakes: 17.5/0.25 (Trim et al., 2005). Numerical simulation results presented by Constantinides and Oakley (2006) for a 15/0.25 configuration are consistent with the experimental tests cited above, where VIV is nearly suppressed.

The frequency response is presented in Fig. 4(b). Each symbol refers to the dominant peak in the spectrum. Two additional lines are shown in each plot: the horizontal line represents the natural frequency, when $f = f_n$ or $f^* = 1$, and the diagonal line represents the vortex-shedding frequency for the static cylinder, also known as Strouhal frequency, when $f = f_{St}$. For the plain cylinder, a similar behaviour found by Khalak and Williamson (1999) for $m^* \approx 2$ is

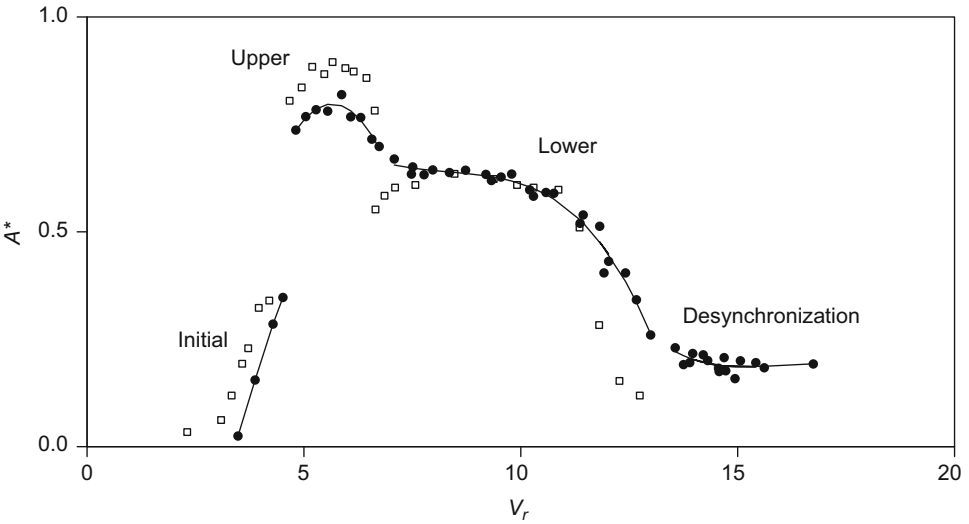

Fig. 3. Amplitude response for an isolated plain cylinder. •, Present data, $m^* = 1.8$ and $m^*\zeta = 0.0081$; □, data compiled by Khalak and Williamson (1999), $m^* = 2.4$ and $m^*\zeta = 0.014$.

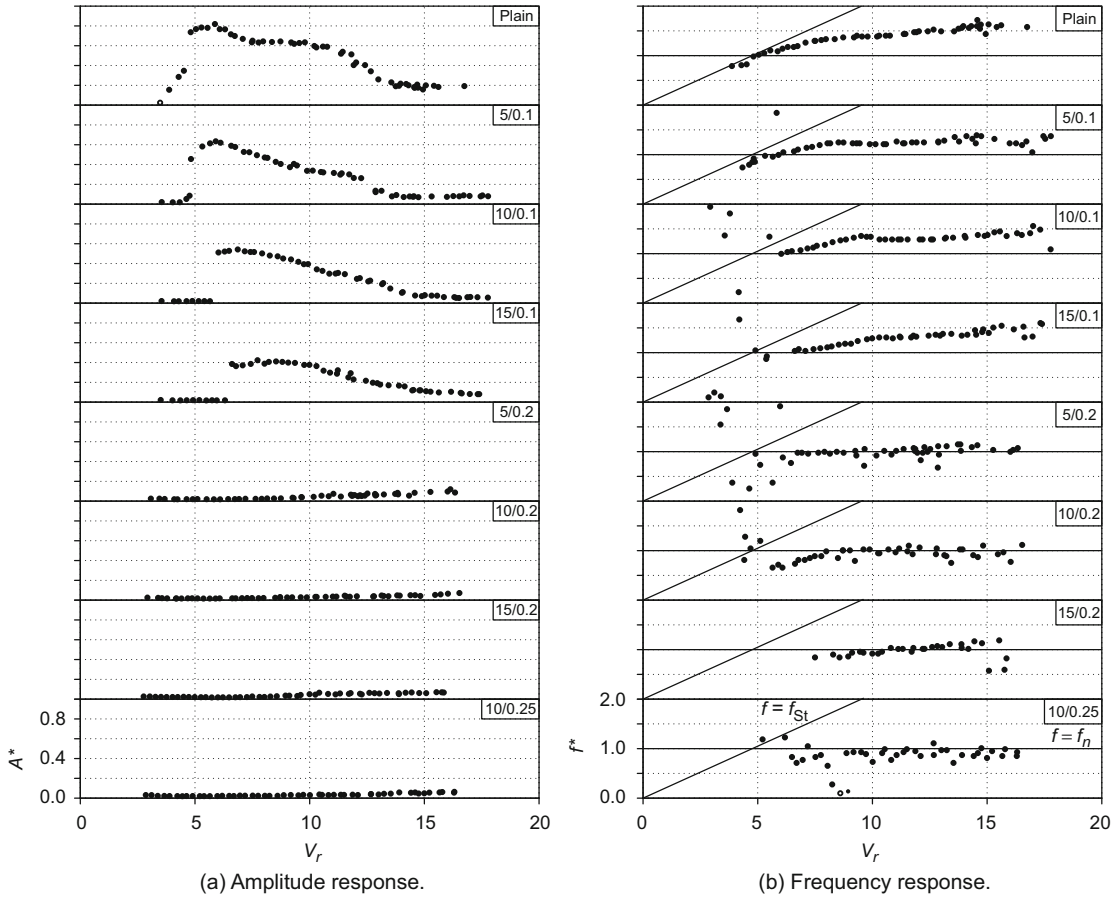

Fig. 4. Amplitude and frequency responses for isolated plain and straked cylinders.

observed. The frequency f^* rises to 1.5 over the synchronization range $V_r = 4$–11 and there is no "lock-in" around $f^* = 1$, which is a result of imposing a low mass ratio. The low-height ($h = 0.1d$) straked cylinders also reach frequency f^* values close to 1.5, but with initial frequencies diverging from the Strouhal frequency f_{St} more promptly as the pitch is increased. On the other hand, frequency f^* remains close to the unity, with some scatter, for the entire range tested in the high-height ($h = 0.2$, $0.25d$) straked cylinders.

The SDPIV measurements are shown for three cylinder configurations: plain, 10/0.1, and 10/0.2. These configurations are representative of the different response behaviours presented in Fig. 4. Three reduced velocities are depicted in Fig. 5 for each configuration. In all cases, the circular cylinder is located at the phase angle ϕ during the cycle of oscillation. The reduced velocities, $V_r = 3$, 6, and 9, correspond to the 2S-initial, 2P-upper, and 2P-lower shedding patterns, respectively, a well-known behaviour of the plain cylinder response (Govardhan and Williamson, 2000). The plain cylinder vorticity and velocity fields are shown in Figs. 5(a), (b), and (c), where a close interaction between the shear layers and the resulting oscillating wake can be observed. The out-of-plane velocity has the same order of magnitude of the flow velocity, $U_z/U = \mathcal{O}(1)$, and the figures show spanwise movements at the same location as the high intensity spanwise vorticity, which can be an indication of the existence of secondary streamwise vortices.

In the straked cylinder cases, the separation of the shear layers is controlled by the strake height, as seen in Figs. 5(d) and (g). At $V_r = 3$, the shear layers of the straked cylinders interact farther from the base region than the shear layers of the plain cylinder. As the V_r is increased, the alternate shedding of vortices in the wake of the 10/0.1 cylinder, shown in Figs. 5(e) and (f), is directly associated with its significant amplitude oscillation. The 10/0.2 cylinder wake width remains constant with the increase in velocity. From the 10/0.2 cylinder figures, one can see that the shear layers do not interact with each other, and the related absence of an oscillating wake results in the suppression of VIV. As with the plain cylinder case, the out-of-plane velocity has a comparable order of magnitude with the flow velocity and its region of

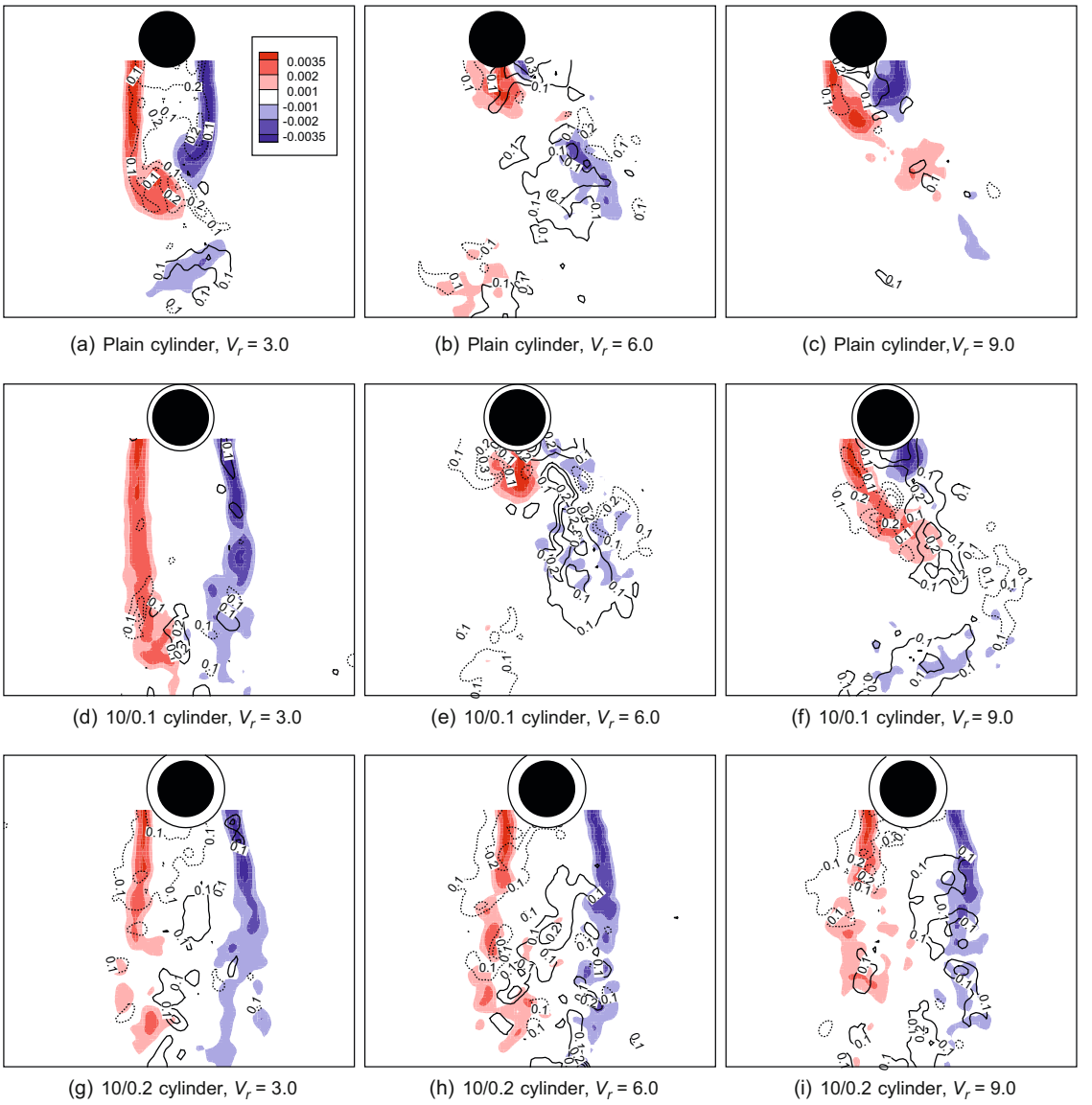

Fig. 5. Phase averaged spanwise vorticity field ($\omega_z d/U$, from negative values in blue, through null in white, to positive ones in red) superposed to phase averaged spanwise velocity field (U_z/U, from negative values in dashed lines to positive one in solid lines) for isolated plain and straked cylinders. The spanwise direction is the out-of-plane direction and the cylinder is located at the phase angle ϕ during the cycle.

higher intensity indicates a constant deflection of the flow in the vicinity of the body due to the presence of the helical strake. Figs. 5(d) and (g) show the effect that the strake height has on the out-of-plane velocity, as it increases the three-dimensionality along the span in a controlled way. Considering the SDPIV section of the flow around a straked cylinder, the strake helices have a certain orientation that result in a preferential (biased) deflection of the spanwise velocity. All figures (Figs. 5(g)–(i)) with the 10/0.2 strake configuration have two notable spanwise velocity structures in the cylinder wake: one negative, attached to the body, and one positive in a position further downstream. These figures clearly show that the effect of the strakes in the flow is the same for the three reduced velocities tested. The flow deflection due to the presence of the strakes affects the vortex formation as the helical configuration disrupts the regular shedding of vortices along the span.

The isolated cylinder SDPIV results indicate that the main effects regarding the efficiency of strakes are the constant width of the wake and the resulting farther interaction between the shear layers, in addition to the controlled three-dimensionality along the span, all which prevent the regular shedding of vortices close to the cylinder base. These dynamic effects are directly related to the height of the strake.

3.2. Tandem cylinders

Fig. 6 presents the amplitude and frequency responses for the flow interaction of an elastically mounted rigid cylinder oscillating in the wake shed from an upstream cylinder. Both cylinders are plain and serve as a benchmark for all subsequent comparisons. For the five gaps tested, the amplitude (Fig. 6(a)) presents two distinct behaviours: the $s/d = 3$, 4, 5 and 6 responses monotonically increase without the typical upper and lower branches of an oscillating single cylinder, while the $s/d = 2$ response reaches an asymptotic amplitude. The continuous increase in the amplitude response to the increasingly reduced velocity is usually found in galloping oscillations, when the upstream body wake interacts with the downstream one generating forces that excite the body in oscillations of high amplitude. The oscillations start around $V_r = 3$ and rise continuously. The highest observed amplitude for all cases is $A^* \simeq 1.25$ and occurs at the maximum reduced velocity ($V_r = 21$). This maximum amplitude is 56% higher than the one measured for the case of the isolated plain cylinder. The maximum amplitude is observed for the $s/d = 3$ gap. Similar results were found by Ássi et al. (2006). However, as one gap displays asymptotic amplitude behaviour, the existence of galloping oscillations cannot be claimed as a reason. As shown in Ássi et al. (2007), the asymptotic oscillation amplitude persists up to $V_r = 35$ with the $s/d = 3$ gap. Consequently, the phenomenon is better described as wake-induced vibrations.

The frequency response is shown in Fig. 6(b), where some differences between each tested gap can be observed. For the first three gaps ($s/d = 2,3,4$), there is a region of lock-in, $f = f_n$, for $3 \leq V_r \leq 6$, and a subsequent increase of the frequency f^*, for $V_r > 6$. The greater gaps ($s/d = 5,6$) present quite a different behaviour in the initial oscillation range,

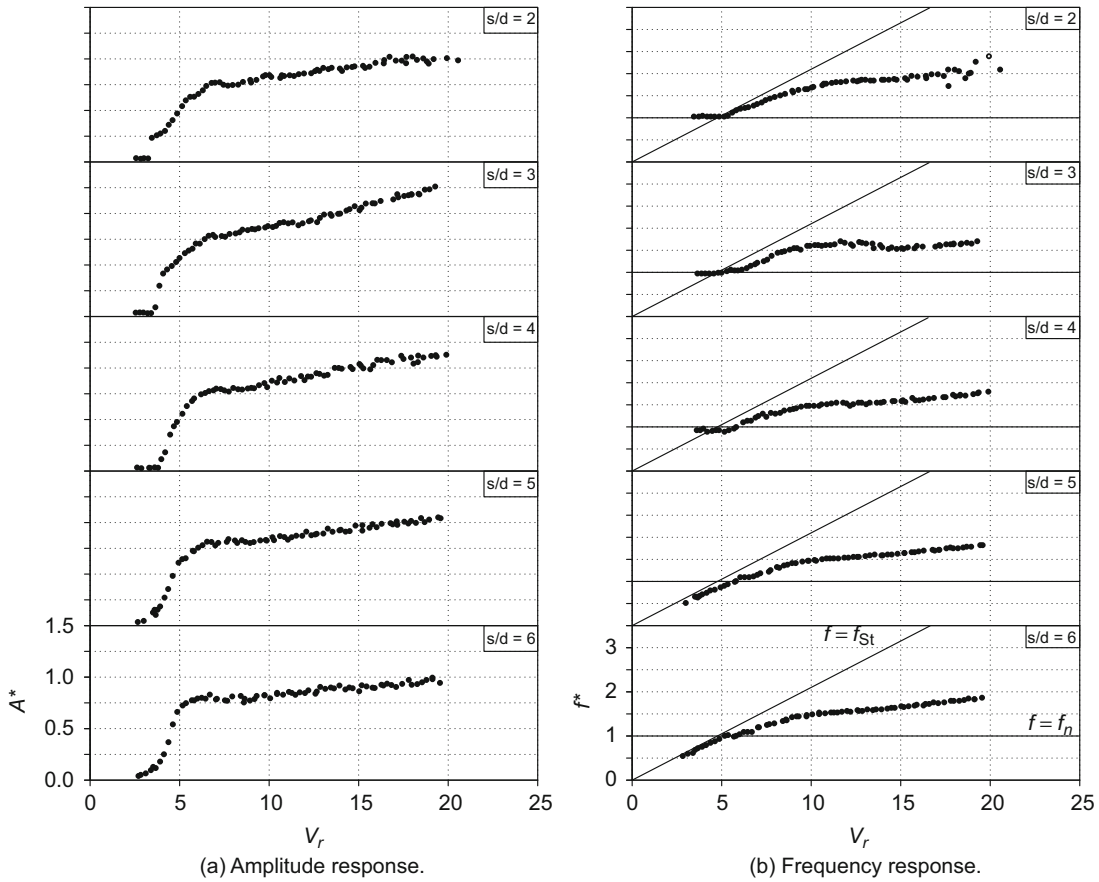

Fig. 6. Amplitude and frequency responses for downstream plain cylinder in tandem.

with $f = f_{St}$, and then an increase in frequency diverging from the Strouhal frequency, a behaviour also noted for the other gaps.

To verify the response of a straked cylinder immersed in the wake of a plain fixed cylinder, the downstream cylinder is fitted with 10/0.2 helical strakes. The 10/0.2 strake configuration is chosen because it yields the lowest amplitude response and it has an intermediate configuration regarding strake pitch and height.

Contrary to the isolated case, the interference tests show that the downstream straked cylinder oscillates significantly, although the oscillatory response is quite different to the case of both plain cylinders. Fig. 7(a) presents the amplitude response for five gaps. As can be seen, the increase of the gap reduces the maximum amplitude response. The reduced velocity where the peak amplitude occurs also decreases, from $V_r = 8$ to 5, with the increase of the gap. The amplitude response of the downstream straked cylinder shows a well-defined peak and then oscillates at a constantly lower amplitude. The increase of the gap reduces both the peak and the oscillation amplitudes for higher reduced velocities. Considering the V_r range tested, it seems that the amplitude reaches an asymptotic value as V_r is increased. For instance, the peak and the asymptotic amplitudes are 0.75 and 0.6, respectively, for the $s/d = 2$ gap; they are reduced to 0.38 and 0.15 for the $s/d = 6$ configuration. This behaviour is very different from that found in the case of the downstream plain cylinder, in which the amplitude of oscillation increases continuously as the reduced velocity is increased for all gaps tested, except $s/d = 2$.

The frequency response for the straked cylinder in tandem is presented in Fig. 7(b), along with three additional lines: the horizontal line represents the natural frequency, when $f = f_n$ or $f^* = 1$, the higher slope diagonal line represents the vortex-shedding frequency for the fixed cylinder, also known as Strouhal frequency, when $f = f_{St}$, and the lower slope diagonal line represents half the Strouhal frequency, $f = f_{St}/2$. The first two gaps ($s/d = 2,3$) show similar behaviour, where there is a small region of lock-in ($f^* = 1$) followed by an increasing frequency parallel to the $f = f_{St}/2$ line. The $s/d = 4$ gap also has a lock-in region up to $V_r = 6$, but it presents an alternating behaviour between half the Strouhal

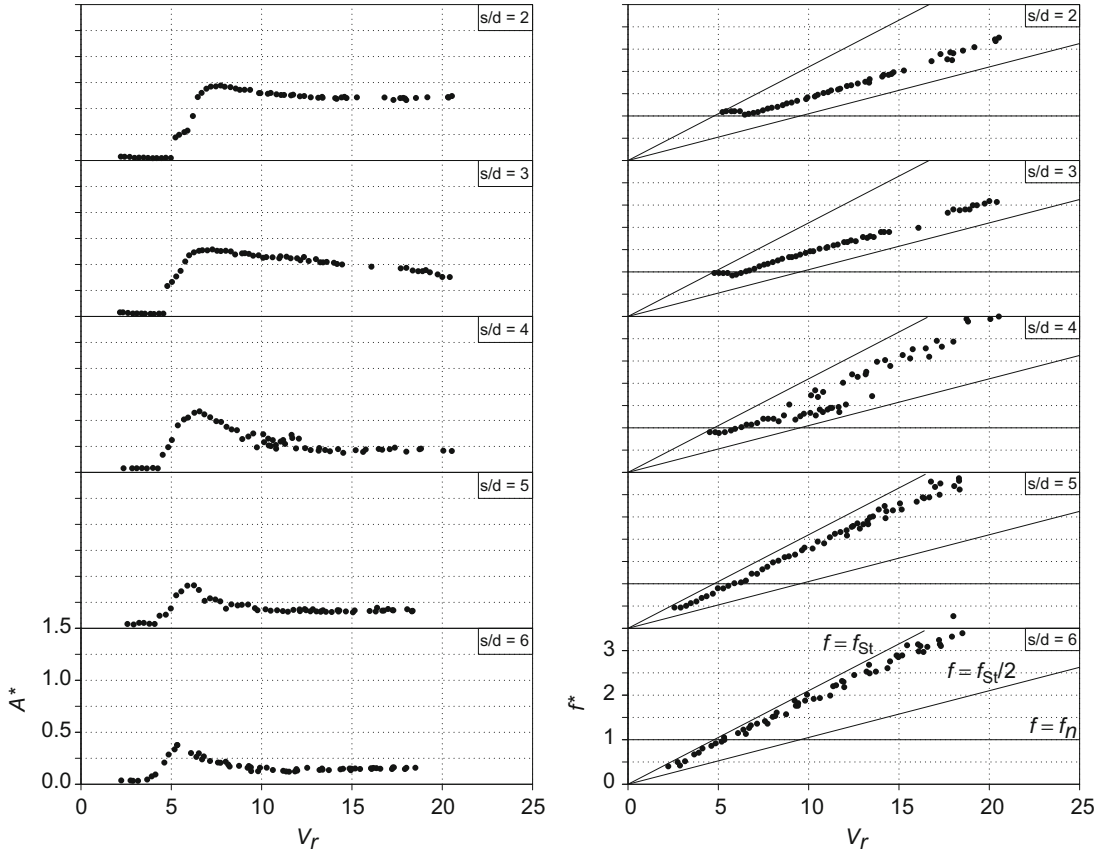

(a) Amplitude response. (b) Frequency response.

Fig. 7. Amplitude and frequency responses for downstream straked (10/0.2) cylinder in tandem.

frequency and the Strouhal frequency up to $V_r = 13$, and then increases parallel to the $f = f_{St}$ line. The other two gaps ($s/d = 5$, 6) follow the $f = f_{St}$ line all the way up to the maximum V_r.

A more comprehensive spectral analysis is conducted in order to investigate the origin of the behaviour of alternating frequency in regarding the $s/d = 4$ gap configuration. Fig. 8 shows the power spectral density ($PSD^* = PSD/PSD_{max}$) for some representative points. Firstly, the spectrum at $V_r = 5.93$ presents one well-defined peak. The next two spectra ($V_r = 10.4$ and 11.3) contain two close dominant frequencies. This fact certainly explains the transition between the frequencies f_{St} and $f_{St}/2$ in the region of $V_r \approx 8-13$ for the $s/d = 4$ case. Finally, taking one point beyond the alternating frequency region ($V_r = 15.2$), the spectrum again shows just one well-defined peak. As a result, the $s/d = 4$ represents an intermediate gap between two distinct responses, one parallel to $f = f_{St}/2$ and the other to $f = f_{St}$.

The downstream cylinder wake measured by SDPIV is presented for the same three reduced velocities ($V_r = 3$, 6, and 9) of the isolated cylinder tests. Three separation values ($s/d = 2$, 4, and 6) are considered as they represent the lower and upper limits tested, and an intermediate gap. An extensive visualization study of the flow between two tandem cylinders was conducted by Ássi (2005) in order to investigate the flow characteristics of this arrangement and how it affects the wake of the downstream cylinder. Additionally, the objective of employing the SDPIV technique in the present study is to investigate the three-dimensionalities of the wake of the downstream cylinder and how this wake differs from the one found in the case of the isolated cylinder.

In the case of both plain cylinders, Fig. 9 shows that the shear layers roll up right after the downstream body resulting in alternating vortex shedding and an oscillatory wake. One can see that the vortex structures are different from those found in the case of the isolated plain cylinder (Fig. 5), notably at $V_r = 3$, where the shear layers roll up at a farther distance for the isolated cylinder, and at $V_r = 9$, where the higher oscillation amplitude of the downstream tandem cylinder generates the first counter-clockwise (positive) vortex elongated in the horizontal direction. It can also be noted that the wake width increases when the gap is increased, a behaviour best seen in Figs. 9(b), (e) and (h). Such a trait may be explained by the different vortex street configurations that exist as a function of the gap between two tandem cylinders. For the stationary tandem cylinder arrangement, Zdravkovich (1985) presented the following classification: one vortex street for gaps $s/d = 1$–3, where both cylinders act as a single body; one bistable regime around $s/d \approx 4$, where there is alternation between one and two vortex streets; and two vortex streets, one for each cylinder, for $s/d > 5$. For the same configuration tested in the present study, Ássi et al. (2006) investigated the effect of the variation of reduced velocity in the flow configuration for a fixed gap. A change from the one vortex street to the regime of two vortex streets was also found as the reduced velocity was increased. As in the wake of the isolated plain cylinder, the greater spanwise velocity values coincide with the spanwise vorticity of high intensity.

Contrary to the isolated 10/0.2 straked cylinder, there is a strong interaction between shear layers from low reduced velocities in the tandem arrangement with a downstream straked cylinder, as seen in Fig. 10. The presence of strong three-dimensionality (spanwise velocity) is also noted at the region of spanwise vorticity of high intensity. Regarding the effect of increasing V_r, for the $s/d = 2$ case, one can observe alternating vortices at $V_r = 9$ that correspond to the high

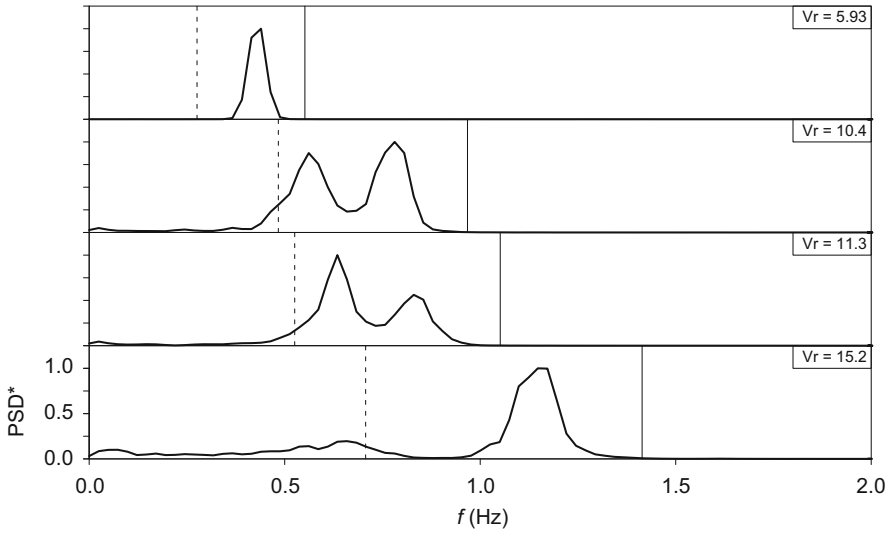

Fig. 8. Spectral analysis for the $s/d = 4$ gap configuration. Solid lines: $f = f_{St}$ and dashed lines: $f = f_{St}/2$.

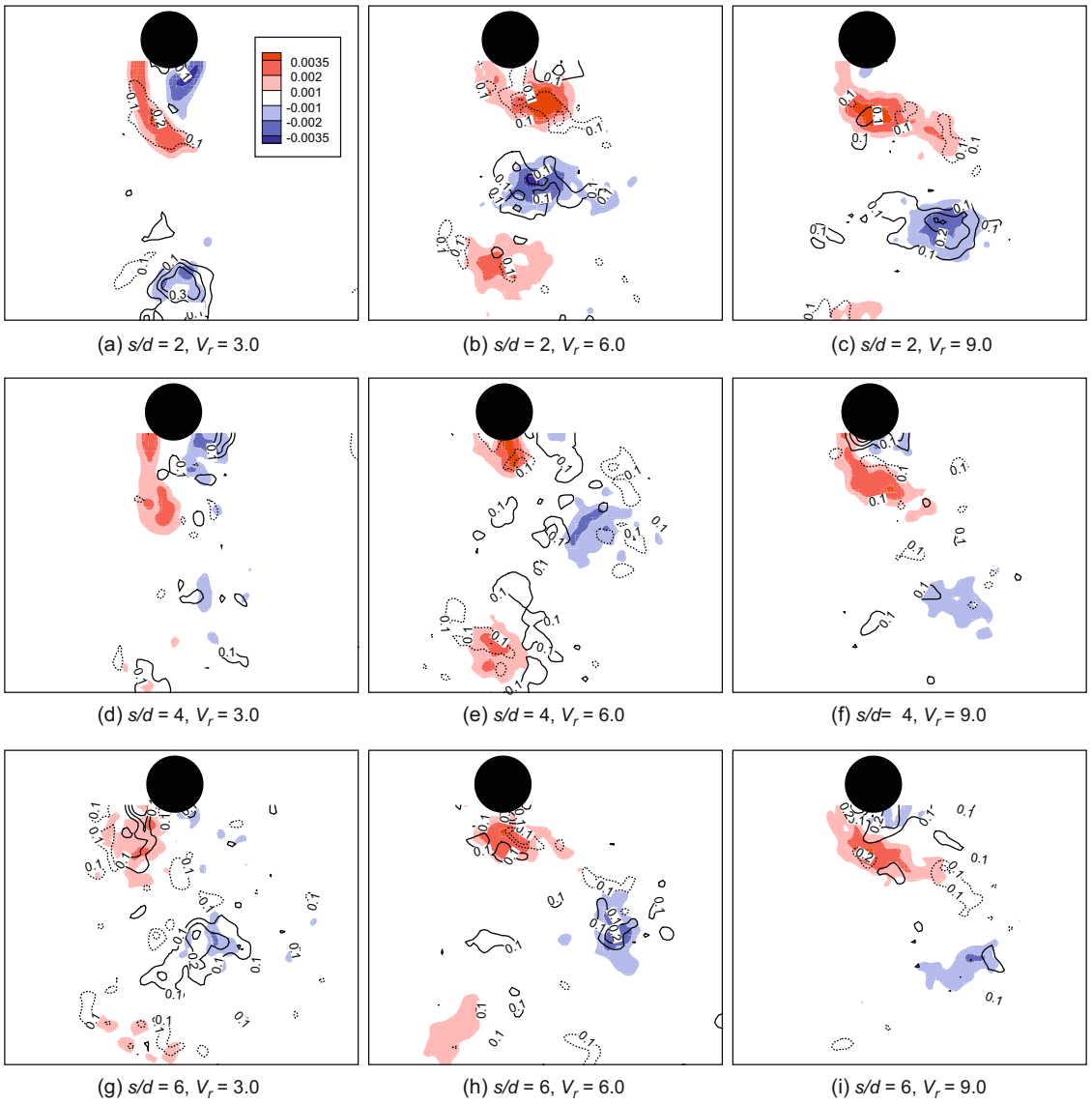

Fig. 9. Phase averaged spanwise vorticity field ($\omega_z d/U$, from negative values in blue, through null in white, to positive ones in red) superposed to phase averaged spanwise velocity field (U_z/U, from negative values in dashed lines to positive one in solid lines) for downstream plain cylinder in tandem. The spanwise direction is the out-of-plane direction and the cylinder is located at the phase angle ϕ during the cycle.

amplitude response found in Fig. 7(a). Again, the modification of the wake patterns is a function of the gap and V_r. For the $s/d = 2$ gap, the V_r increase changes the flow pattern with two slightly separated shear layers to the shedding of alternating vortices. On the other hand, the increase from $V_r = 6$ to 9 results in a modification from an alternating vortex shedding pattern to an apparently separated shear layer wake for $s/d = 4$ and 6. The effect of this change of wake pattern can be seen in the amplitude response in Fig. 7(a), where the amplitude of the oscillation peak around $V_r = 6$ decreases to asymptotic values for $V_r > 9$. Considering the gap increase, the $V_r = 9$ flow fields are good examples of the modifications of flow pattern and the related differences in dynamic responses. The alternating vortex shedding found for $s/d = 2$ (Fig. 10(c)) changes to two separated shear layers for $s/d = 4$ (Fig. 10(f)), and this trait is intensified for $s/d = 6$ (Fig. 10(i)).

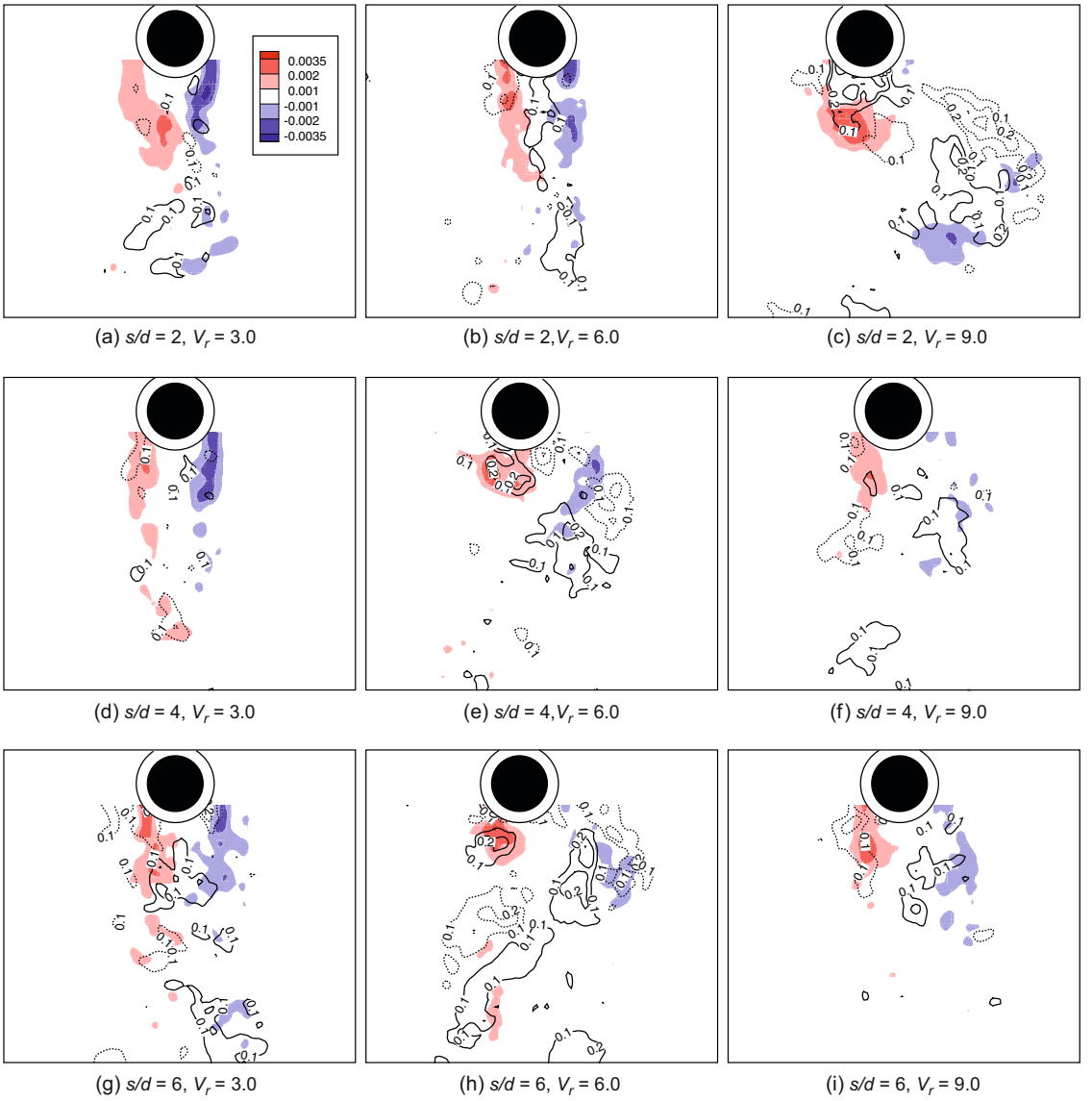

Fig. 10. Phase averaged spanwise vorticity field ($\omega_z d/U$, from negative values in blue, through null in white, to positive ones in red) superposed to phase averaged spanwise velocity field (U_z/U, from negative values in dashed lines to positive one in solid lines) for downstream straked (10/0.2) cylinder in tandem. The spanwise direction is the out of the plane direction and the cylinder is located at the phase angle ϕ during the cycle.

4. Conclusions

4.1. Amplitude and frequency responses

The results of the isolated cylinder tests show the importance of the strake height to VIV attenuation/suppression. The $h = 0.1d$ strakes moderately attenuate the amplitude response compared to the plain cylinder. For the $h = 0.1d$ cylinders, the increase in pitch reduces the maximum amplitude response and delays the beginning of the maximum amplitude range. The VIV is almost completely suppressed for the straked cylinders with $h = 0.2d$, and $0.25d$ heights. However, the change of pitch has no apparent effect on the high-height strakes. The frequency response is also affected

by changes in height and pitch, as the low-height strakes have a similar frequency response to the plain cylinder, and the high-height strake frequency f^* stays close to one for the entire range tested.

As found by other researchers, the amplitude response monotonically increases for both plain cylinders in a tandem configuration for the gaps tested, except the $s/d=2$ gap, which reaches an asymptotic amplitude. This continuous increase in the amplitude response with the increase of V_r is commonly found in wake interference oscillations. The frequency response is affected by changing the s/d gap. As the gap is increased, the response of the isolated plain cylinder is recovered.

Although significant oscillations exist for the straked cylinder in tandem, they are bounded and lower than those observed for the isolated and tandem plain cylinder cases. The increase of the gap reduces the maximum and the asymptotic oscillation amplitudes for higher V_r. Regarding the frequency response, the general behaviour is different from the plain cylinder case. The $s/d=2$ and 3 gaps have a small range of synchronization ($f^*=f_n$), followed by a frequency response parallel to $f=f_{St}/2$. The $s/d=4$ gap has an alternating region between $f=f_{St}/2$ and $f=f_{St}$, that contains two close dominant oscillation frequencies. After the alternating region, the frequency rises parallel to $f=f_{St}$. Finally, the $s/d=5$ and 6 frequency responses follow the $f=f_{St}$ frequency up to the maximum V_r.

4.2. SDPIV spanwise vorticity and velocity fields

SDPIV results show a close interaction between the shear layers and a resulting oscillating wake for the plain cylinder. The spanwise (out-of-plane) velocity fields have their higher intensities located at the same position of the spanwise vorticity of high intensity. The alternating values of the spanwise velocity indicate circulating movements that can be an evidence of secondary streamwise vorticity. In the straked cylinders, the shear layer separation is controlled by the strake height, and they interact at a farther distance from the body than the plain cylinder case. The flow visualization for the 10/0.1 cylinder at higher reduced velocities ($V_r=6$ and 9) shows an oscillatory vortex shedding and wake. Such behaviour is directly related to the oscillations of significant amplitude found in low-height straked and plain cylinders. For the 10/0.2 cylinder, the wake width remains constant with the increase in reduced velocity and the shear layers do not interact close to the body. The out-of-plane velocity also has the same order of magnitude as the flow velocity. There is not the expected substantial increase in the intensity of the straked cylinder out-of-plane velocity compared to the plain cylinder. The controlled deflection of the spanwise velocity (three-dimensionality) by the strakes in the wake can prevent the vortex shedding from becoming correlated along the span. Other dynamic effects directly related to the strake height are the width of the wake and the distance of shear layers interaction.

Although one can observe alternating vortex shedding and oscillatory wake, there are some important differences between the isolated plain and both plain cylinders in tandem. In the tandem configuration, the shear layers roll up closer to the body and the width of the wake increases as the separation gap is increased. The increases in the gap and reduced velocity are responsible for the differences between the wake visualization results. Other researchers have investigated these effects and their results indicate the existence of one vortex street for both bodies; two vortex streets, one for each body, and an alternating region between one and two vortex streets. The change between the flow regimes can be observed separately with the increase in the gap or reduced velocity. The spatial coincidence between the higher values of spanwise velocity and vorticity is observed for both the isolated and tandem plain cylinder cases.

Contrary to the isolated 10/0.2 straked cylinder, there is a strong interaction between the shear layers in the tandem arrangement for low reduced velocities. From the SDPIV results, it is possible to observe alternating vortex shedding and a resulting oscillating wake for the plain/straked tandem arrangement. As already noted for the configuration of two plain cylinders in tandem, the changes of gap and reduced velocity significantly modify the wake pattern. Basically, the wake pattern changes from alternating vortex shedding to separated shear layers as the gap or the reduced velocity are increased. The flow fields show that the change of wake pattern can be obtained separately either by the gap or the V_r increase. Naturally, the amplitude response is affected by the change of wake pattern, where the alternating vortex shedding is associated with high amplitude oscillations, while the separated shear layers are found in oscillatory motions of low amplitude. The location of higher spanwise velocities coincides with the region of strong spanwise vorticity, a characteristic also found in the other configurations tested.

4.3. Final remarks

Despite the dramatic change of the flow characteristics when the straked cylinder is immersed in an oscillating wake, the 10/0.2 strake configuration is still efficient for $s/d \geq 4$ and $V_r > 10$ with regard to the oscillation amplitude, specially when compared to the plain cylinder cases in both isolated and tandem arrangements.

Acknowledgements

The authors are grateful to FINEP-CTPetro, CNPq, and Petrobras for providing them a research grant for this project. I.K. would also like to acknowledge FAPESP for the scholarship provided during the development of this work and to Maria Cristina Vidal Borba and David Sweetman for advice regarding the English language. All experimental resources were provided by NDF-USP.

References

Alam, M.M., Moriya, M., Takai, K., Sakamoto, H., 2003. Fluctuating fluid forces acting on two circular cylinders in a tandem arrangement at a subcritical Reynolds numbers. Journal of Wind Engineering and Industrial Aerodynamics 91, 139–154.

Ássi, G.R.S., 2005. Estudo experimental do efeito de interferência no escoamento ao redor de cilindros alinhados. Master's Thesis, EPUSP, São Paulo.

Ássi, G.R.S., Bearman, P.W., Kitney, N., 2009. Low drag solutions for suppressing vortex-induced vibration of circular cylinders. Journal of Fluids and Structures 25, 666–675.

Ássi, G.R.S., Bearman, P.W., Meneghini, J.R., 2007. Dynamic response of a circular cylinder in the wake of an upstream fixed cylinder. In: Leweke, T., Meneghini, J.R., Williamson, C.H.K. (Eds.), Proceedings of the Fifth Conference on Bluff Body Wakes and Vortex-Induced Vibrations, BBVIV, Costa do Sauípe, Bahia, Brazil.

Ássi, G.R.S., Meneghini, J.R., Aranha, J.A.P., Bearman, P.W., Casaprima, E., 2006. Experimental investigation of flow-induced vibration interference between two circular cylinders. Journal of Fluids and Structures 22, 819–827.

Bearman, P.W., 1984. Vortex shedding from oscillating bluff bodies. Annual Review of Fluid Mechanics 16, 195–222.

Bearman, P.W., Branković, M., 2004. Experimental studies of passive control of vortex-induced vibration. European Journal of Mechanics—B: Fluids 23, 9–15.

Bearman, P.W., Owen, J.C., 1998. Reduction of bluff-body drag and suppression of vortex shedding by the introduction of wavy separation lines. Journal of Fluids and Structures 12, 123–130.

Bokaian, A., Geoola, F., 1984. Wake-induced galloping of two interfering circular cylinders. Journal of Fluid Mechanics 146, 383–415.

Branković, M., Bearman, P.W., 2006. Measurements of transverse forces on circular cylinders undergoing vortex-induced vibration. Journal of Fluids and Structures 22, 829–836.

Brika, D., Laneville, A., 1999. The flow interaction between a stationary cylinder and a downstream flexible cylinder. Journal of Fluids and Structures 13, 579–606.

Carmo, B.S., Meneghini, J.R., 2006. Numerical investigation of the flow around two circular cylinders in tandem. Journal of Fluids and Structures 22, 979–988.

Carmo, B.S., Meneghini, J.R., Sherwin, S.J., 2010. Secondary instabilities in the flow around two circular cylinders in tandem. Journal of Fluid Mechanics 644, 395–431.

Carmo, B.S., Sherwin, S.J., Bearman, P.W., Willden, R.H.J., 2008. Wake transition in the flow around two circular cylinders in staggered arrangements. Journal of Fluid Mechanics 597, 1–29.

Choi, H., Jeon, W.-P., Kim, J., 2008. Control of flow over a bluff body. Annual Review of Fluid Mechanics 40, 113–139.

Constantinides, Y., Oakley, O.H., 2006. Numerical prediction of bare and straked cylinder VIV. In: Kuehnlein, W.L., Valentine, D. (Eds.), Proceedings of 25th International Conference on Offshore Mechanics and Artic Engineering, OMAE, Hamburg, Germany.

Galvao, R., Lee, E., Farrell, D., Hover, F., Triantafyllou, M., Kitney, N., Beynet, P., 2008. Flow control in flow-structure interaction. Journal of Fluids and Structures 24, 1216–1226.

Govardhan, R., Williamson, C.H.K., 2000. Modes of vortex formation and frequency response of a freely vibrating cylinder. Journal of Fluid Mechanics 420, 85–130.

Hanson, R., Mohany, A., Ziada, S., 2009. Flow-excited acoustic resonance of two side-by-side cylinders in cross-flow. Journal of Fluids and Structures 25, 80–94.

Hover, F.S., Triantafyllou, M.S., 2001. Galloping response of a cylinder with upstream wake interference. Journal of Fluids and Structures 15, 503–512.

Khalak, A., Williamson, C.H.K., 1999. Motions forces and mode transitions in VIV at low mass-damping. Journal of Fluids and Structures 13, 813–851.

Korkischko, I., Meneghini, J.R., Casaprima, E., Franciss, R., 2007a. An experimental investigation of the flow around isolated and tandem straked cylinders. In: Leweke, T., Meneghini, J.R., Williamson, C.H.K. (Eds.), Proceedings of the Fifth Conference on Bluff Body Wakes and Vortex-Induced Vibrations, BBVIV, Costa do Sauípe, Bahia, Brazil.

Korkischko, I., Meneghini, J.R., Gioria, R.S., Jabardo, P.J., Casaprima, E., Franciss, R., 2007b. An experimental investigation of the flow around straked cylinders. In: Halkyard, J., Yim, S.C. (Eds.), Proceedings of 26th International Conference on Offshore Mechanics and Artic Engineering, OMAE, San Diego, USA.

Laneville, A., Brika, D., 1999. The fluid and mechanical coupling between two circular cylinders in tandem arrangement. Journal of Fluids and Structures 13, 967–986.

Li, H., Sumner, D., 2009. Vortex shedding from two finite circular cylinders in a staggered configuration. Journal of Fluids and Structures 25, 479–505.

Meneghini, J.R., Saltara, F., Siqueira, C.L.R., Ferrari Jr., J.A., 2001. Numerical simulation of flow interference between two circular cylinders in tandem and side-by-side arrangements. Journal of Fluids and Structures 15, 327–350.

Mizushima, J., Ino, Y., 2008. Stability of flows past a pair of circular cylinders in a side-by-side arrangements. Journal of Fluid Mechanics 595, 491–507.

Papaioannou, G.N., Yue, D.K.P., Triantafyllou, M.S., Karniadakis, G.E., 2008. On the effect of spacing on the vortex-induced vibrations of two tandem cylinders. Journal of Fluids and Structures 24, 833–854.

Parkinson, G., 1989. Phenomena and modelling of flow-induced vibrations of bluff bodies. Progress in Aerospace Sciences (26), 169–224.

Prasad, A.K., 2000. Stereoscopic particle image velocimetry. Experiments in Fluids 29, 103–116.

Prasanth, T.K., Mittal, S., 2009. Flow-induced oscillation of two circular cylinders in tandem arrangement at low Re. Journal of Fluids and Structures 25, 1029–1048.

Rocchi, D., Zasso, A., 2002. Vortex shedding from a circular cylinder in a smooth and wired configuration: comparison between 3D LES simulation and experimental analysis. Journal of Wind Engineering and Industrial Aerodynamics 90, 475–489.

Sarpkaya, T., 1979. Vortex-induced oscillations. Journal of Applied Mechanics 46, 241–258.

Simantiras, P., Willis, N., 1999. Investigation on vortex-induced oscillations and helical strakes effectiveness at very high incidence angles. In: Chung, J.S. (Ed.), Proceedings of the Ninth International Offshore and Polar Engineering Conference, ISOPE, Brest, France.

Sumner, D., Price, S.J., Padoussis, M.P., 2000. Flow-pattern identification for two staggered circular cylinders in cross-flow. Journal of Fluid Mechanics 411, 263–303.

Trim, A.D., Braaten, H., Lie, H., Tognarelli, M.A., 2005. Experimental investigation of vortex-induced vibration of long marine risers. Journal of Fluids and Structures 21, 335–361.

Willden, R.H.J., Graham, J.M.R., 2001. Numerical prediction of VIV on long flexible circular cylinders. Journal of Fluids and Structures 15, 659–669.

Williamson, C.H.K., Govardhan, R.N., 2004. Vortex-induced vibrations. Annual Review of Fluid Mechanics 36, 413–455.

Zdravkovich, M.M., 1981. Review and classification of various aerodynamic and hydrodynamic means for suppressing vortex shedding. Journal of Wind Engineering and Industrial Aerodynamics 7, 145–189.

Zdravkovich, M.M., 1984. Reduction of effectiveness of means for suppressing wind-induced oscillation. Engineering Structures 6, 344–349.

Zdravkovich, M.M., 1985. Flow induced oscillations of two interfering circular cylinders. Journal of Sound and Vibrations 101, 511–521.